Inorganic Chemistry

ARTICLE

pubs.acs.org/IC

Synthesis, Structure, and Photoluminescent Properties of Metal–Organic Coordination Polymers Assembled with Bithiophenedicarboxylic Acid

Jiao Zhao,[†,‡] Xiu-Li Wang,[†,‡] Xin Shi,[§] Qi-Hua Yang,[*,†] and Can Li[*,†]

[†]State Key Laboratory of Catalysis, Dalian Institute of Chemical Physics, Chinese Academy of Sciences, 457 Zhongshan Road, Dalian 116023, China

[‡]Graduate School of the Chinese Academy of Sciences, Beijing 100049, China

[§]Institute of Chemistry for Functionalized Materials, Department of Chemistry & Chemical Engineering, Liaoning Normal University, 850 Huanghe Road, Dalian 116029, China

Supporting Information

ABSTRACT: Four novel metal–organic coordination polymers with the formulas $Mn_3(btdc)_3(DMF)_4$ (**1**), $Co(btdc)(DMF)_3$ (**2**), $Zn(btdc)(DMF)_3$ (**3**), and $Zn(btdc)(4,4'\text{-bpy})_{0.5}$ (**4**), where H_2btdc = 2,2′-bithiophene-5,5′-dicarboxylic acid, DMF = *N*,*N*′-dimethylformamide, and 4,4′-bpy = 4,4′-bipyridine, have been successfully synthesized. Crystal **1** with Mn^{2+} as the cation features a three-dimensional (3D) infinite framework built from trimanganese clusters, and crystals **2** and **3** with Co^{2+} and Zn^{2+}, respectively, as the cation both have one-dimensional zigzag polymeric coordination chains. Crystal **4** synthesized using a mixture of 4,4′-bpy and H_2btdc exhibits a triply interpenetrating 3D framework built from a dizinc paddlewheel second building unit with a distorted primitive cubic single net. The results of UV/vis spectra indicate that metal binding does not disturb the detailed electronic structure of the ligand. We also demonstrate that Zn^{2+} can greatly enhance the luminescence emission of the H_2btdc ligand, and the emission intensity of crystal **4** is almost 20 times higher than that of the free H_2btdc ligand. Steady-state and time-resolved spectroscopic measurement reveal that the more rigid environment of the btdc ligand can stabilize the highly excited long-lived states in metal–organic frameworks (MOFs), which thus greatly changes the emission properties of MOFs.

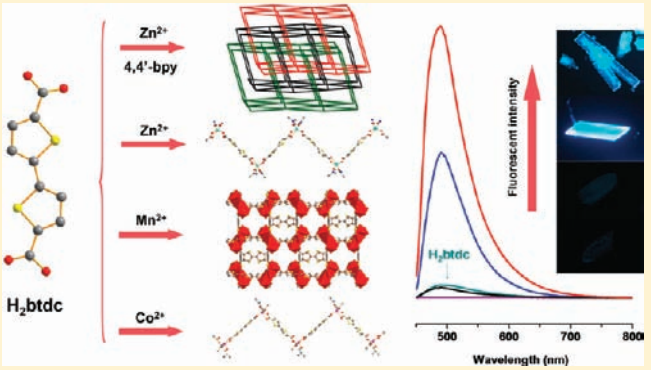

1. INTRODUCTION

Metal–organic coordination polymers, also known as metal–organic frameworks (MOFs) are metal–ligand hybrid compounds that extend into one, two, or three dimensions via a coordination bond. These compounds are built from inorganic connectors (metal ions or polynuclear clusters) and organic ligand linkers.[1] A wide variety of interesting structures are accessible, depending on a number of factors including the connectivity, charge, geometry of the connectors and linkers, nature of the coordinating sites, and length of the linkers.

The functionalized MOFs have attracted much attention in recent years because of not only their enormous variety of interesting structural topologies but also their wide potential applications as functional materials, such as gas adsorption and separation,[2] luminescence,[3] magnetism,[4] host–guest chemistry,[5] catalysis,[6] and so on. Compared with the adsorption properties of MOFs, the photoelectric properties of MOFs are not well investigated.[7−9] MOFs with easily tunable structure and composition may be promising luminescent materials because both the metal and ligand can be used to generate luminescence. Studies on the investigation of the luminescent properties of MOFs are still in their infancy. Roughly, the luminescent MOF can be catalogued into ligand-based emission and metal-ion-centered luminescence. The MOFs displaying ligand-based emission have the advantages of readily tuned emission properties through changes in the nature of the linker and/or structure of the MOFs.[10,11] The synthesis of novel MOFs with ligand-based emission properties should be very interesting.

Bithiophenedicarboxylic acid has interesting photoelectric properties. The structural, optical, and electrochemical properties of the thiophene-based derivatives vary considerably depending on the π-conjugation modes at the thiophene subunits. Therefore, oligo/polythiophene may be a highly promising platform for the construction of a new class of optoelectrochemical materials. Additionally, thiophene is commonly employed as

Received: June 2, 2010
Published: March 11, 2011

Chart 1. Structure of H_2btdc

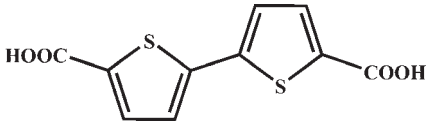

a backbone motif in organic photovoltaic cells and may be considered as the fundamental unit of the electro- and photoluminescent conjugated polymers poly(3-hexylthiophene) (P3HT) and poly(9,9-dioctylfluorene-*co*-bithiophene) (F8T2).[12] Though several coordination polymers have been obtained using the 2,5-thiophenedicarboxylic acid (H_2tdc) ligand,[13,14] the oligothiophenedicarboxylic acid has seldom been employed for the synthesis of MOFs.[15]

In this paper, we report the synthesis and structures of four metal−organic coordination polymers using bithiophenedicarboxylic acid (2,2′-bithiophene-5,5′-dicarboxylic acid, H_2btdc, as shown in Chart 1) as linkers and divalent transitional-metal ions (Mn, Co, and Zn) as connecters. 4,4′-Bipyridine, which is widely employed for the synthesis of MOFs with varied structure, is also used as a colinker to tune the structure of the MOFs. The photoluminescent properties are investigated in detail. The crystals display ligand-based emission properties. We demonstrate that the metal ion and structure both play important roles in the luminescent properties of MOFs. Steady-state and time-resolved spectroscopic measurement reveal that the more rigid environment of the btdc ligand can stabilize the highly excited long-lived states in MOFs, which thus greatly enhanced the emission intensity.

2. EXPERIMENTAL SECTION

2.1. Materials and General Methods. The reagents and solvents employed were commercially available and used as received. 2,2′-Bithiophene-5,5′-dicarboxylic acid (H_2btdc) was synthesized by literature methods (Supporting Information).[15] Elemental analyses were determined on a Vario ELIII elemental analyzer. FT-IR spectra were recorded using KBr disks on a Nicolet Impact 410 spectrophotometer in the range 4000−400 cm^{-1}. The solid-state diffuse-reflectance UV/vis spectra for powder samples were recorded on a Shimadzu UV-2550 UV/vis spectrophotometer equipped with an integrating sphere by using $BaSO_4$ as a white standard. The photoluminescence spectra were measured in a FLS920 fluorescence spectrometer (Edinburgh Instruments, Livingston, U.K.). Time-resolved fluorescence spectra were recorded using the time-correlated single-photon-counting method. The excitation source is a picosecond pulsed diode laser at 406.8 nm with a pulse width of 64.2 ps. Fluorescent microscopy images were obtained using a fluorescence microscope (Nikon TE2000-E). Powder X-ray diffraction (PXRD) data were collected on a Rigaku D/Max-2500PC diffractometer with Cu Kα radiation (λ = 1.5418 Å) over the 2θ range of 5−70° with a scan speed of 5°/min at room temperature. Thermogravimetric analysis (TGA) was performed under an air atmosphere with a heating rate of 5 °C/min by using a NETZSCH STA-449F3 thermogravimetric analyzer.

2.2. Synthesis of the Compounds. *Synthesis of Mn_3(btdc)$_3$-(DMF)$_4$ (**1**).* A mixture of $MnCl_2 \cdot 4H_2O$ (0.2 mmol, 0.0396 g), H_2btdc (0.2 mmol, 0.0508 g) in *N*,*N*′-dimethylformamide (DMF; 7 mL), and anhydrous ethanol (8 mL) was stirred for 10 min in air to form a solution, the solution was placed in a Teflon-lined stainless steel vessel (40 mL), and then the vessel was sealed and heated at 100 °C for 2 days. After the mixture was slowly cooled to room temperature, the yellow crystals of **1** were collected by filtration and washed with DMF (yield: 60% based on Mn). Elem anal. Calcd for $C_{42}H_{40}Mn_3N_4O_{16}S_6$: C, 41.5; H, 3.29; N, 4.61. Found: C, 40.0; H, 3.04; N, 3.15. FT-IR spectrum (cm^{-1}): 1544(s), 1514(s), 1433(s), 1386(s), 1130(w), 1044(w), 772(m).

*Synthesis of Co(btdc)(DMF)$_3$ (**2**).* Crystals of **2** were formed by a liquid diffusion method. A solution of $CoSO_4 \cdot 7H_2O$ (0.1 mmol, 0.0281 g) in DMF (2 mL) was layered at the bottom of the test tube, and then 2 mL of blank DMF was layered at the middle as a buffer layer. Finally, a solution of H_2btdc (0.1 mmol, 0.0254 g) in DMF (3 mL) and anhydrous ethanol (2 mL) was slowly added onto the top. The solutions were left for about 1 week at room temperature, and the purple crystals of **2** were obtained at the interface and bottom layers (yield: 35% based on Co). Elem anal. Calcd for $C_{19}CoH_{25}N_3O_7S_2$: C, 43.0; H, 4.75; N, 7.92. Found: C, 42.5; H, 4.47; N 7.73. FT-IR spectrum (cm^{-1}): 1555(s), 1515(s), 1435(s), 1382(s), 1251(w), 1107(w), 1052(w), 769(m).

*Synthesis of Zn(btdc)(DMF)$_3$ (**3**).* Crystals of **3** were also formed by a liquid diffusion method. A total of 2 mL of an aqueous solution of $Zn(NO_3)_2 \cdot 6H_2O$ (0.1 mmol, 0.0297 g) was layered at the bottom, and then 2 mL of blank DMF was layered at the middle as a buffer layer. H_2btdc (0.2 mmol, 0.0508 g) in DMF (5 mL) was slowly added onto the top. The solutions were left for about 1 week at room temperature, and the light-yellow crystals of **3** were obtained at the interface and bottom layers (yield: 45% based on Zn). Elem anal. Calcd for $C_{19}H_{25}N_3O_7S_2Zn$: C, 42.5; H, 4.69; N, 7.83. Found: C, 41.6; H, 4.37; N, 6.98. FT-IR spectrum (cm^{-1}): 1557(s), 1519(s), 1433(s), 1371(s), 1282(w), 1118(w), 1053(m), 889(w), 833(w), 806(w), 764(m).

*Synthesis of Zn(btdc)(4,4′-bpy)$_{0.5}$ (**4**).* A solution of $Zn(NO_3)_2 \cdot 6H_2O$ (0.2 mmol, 0.0594 g), H_2btdc (0.2 mmol, 0.0508 g), 4,4′-bpy (0.2 mmol, 0.0384 g), DMF (20 mL), and tetrahydrofuran (5 mL) was placed in a Teflon-lined stainless steel vessel (40 mL), and then the vessel was sealed and heated at 85 °C for 1 day. After the mixture was slowly cooled to room temperature, light-yellow crystals of **4** were obtained (yield: 75% based on Zn). Elem anal. Calcd for $C_{15}H_8NO_4S_2Zn$: C, 45.5; H, 2.02; N, 3.54. Found: C, 44.8; H, 2.86; N 3.84. FT-IR spectrum (cm^{-1}): 1629(s), 1520(s), 1430(s), 1384(s), 1214(w), 1070(m), 804(m), 765(s), 642(s).

2.3. X-ray Crystallography. Suitable single crystals of **1**−**4** were mounted onto thin glass fibers in air. The X-ray diffraction data of crystals **1** and **3** were collected on a Bruker Smart CCD diffractometer with graphite-monochromated Mo Kα radiation (λ = 0.710 73 Å) at room temperature, while the data of crystal **2** were collected on an Oxford Diffraction Gemini S Ultra CCD diffractometer at 150 K. The data of crystal **4** were collected on an Oxford Diffraction Gemini S Ultra CCD diffractometer with mirror Cu Kα radiation (λ = 1.541 84 Å) at room temperature. The structures were solved by direct methods and refined by a full-matrix least-squares method against F^2 (*SHELXTL-97*). All non-hydrogen atoms were refined anisotropically. Hydrogen atoms of organic ligands were located geometrically. For crystal **4**, there were large void spaces, and the void spaces were full of disordered solvent molecules. It was difficult to confirm the molecules so that SQUEEZE routine of *PLATON* was used to delete the corresponding Q peaks. On the basis of the TGA results of crystal **4**, there may be two DMF molecules in the unit cell. A summary of the crystallographic data, data collection, and refinement parameters for crystals **1**−**4** are summarized in Table 1. Select bond lengths and angles are listed in Tables 2−5. CCDC reference numbers of crystals **1**−**4** are 779086−779089, respectively. These data can be obtained free of charge from the Cambridge Crystallographic Data Centre via www.ccdc.cam.ac.uk.

3. RESULTS AND DISCUSSION

3.1. Structure Description of the Compounds. *Compound **1**.* X-ray crystallography reveals that crystal **1** has a three-dimensional (3D) framework crystallized in space group *C*2/*c*. There are two crystallographically independent manganese(II) atoms

dx.doi.org/10.1021/ic101112b |*Inorg. Chem.* 2011, 50, 3198–3205

Table 1. Crystal Data and Structure Refinement for Crystals 1−4

crystals	1	2	3	4
formula	$C_{42}H_{40}Mn_3N_4O_{16}S_6$	$C_{19}CoH_{25}N_3O_7S_2$	$C_{19}H_{25}N_3O_7S_2Zn$	$C_{15}H_8NO_4S_2Zn$
fw	1213.96	530.47	536.91	395.71
cryst syst	monoclinic	monoclinic	monoclinic	monoclinic
space group	$C\,2/c$	$P\,2_1/c$	$P\,2_1/c$	$C\,2/c$
a/Å	18.7201(9)	6.5472(1)	6.593(1)	17.7608(4)
b/Å	15.0754(8)	22.5911(5)	22.791(4)	21.7728(4)
c/Å	19.425(1)	16.3206(3)	16.307(3)	9.4874(2)
α/deg	90	90	90	90
β/deg	106.241(3)	92.668(2)	92.755(3)	109.188(2)
γ/deg	90	90	90	90
V/Å^3	5263.2(5)	2411.34(8)	2447.7(8)	3464.98(1)
Z	4	4	4	8
D_c /g cm^{-3}	1.532	1.461	1.457	1.517
μ/mm^{-1}	1.015	0.928	1.217	4.380
F(000)	2476	1100	1112	1592
unique reflns	5888	4928	5541	3206
R_{int}	0.0607	0.0224	0.0658	0.0225
R1 [$I > 2\sigma(I)$]	0.0835	0.0354	0.0481	0.0387
wR2 (all data)	0.2890	0.0824	0.0894	0.1080

Table 2. Select Bond Lengths [Å] and Angles [deg] for Crystal 1[a]

Mn1−O8	2.125(6)	Mn1−O4	2.141(5)
Mn1−O1	2.222(5)	Mn2−O2	2.304(6)
Mn2−O3	2.087(6)	Mn2−O7	2.125(8)
Mn2−O6	2.139(6)	Mn2−O5	2.231(8)
Mn2−O1	2.281(6)		
O8^i−Mn1−O8	180.000(1)	O4^i−Mn1−O4	180.000(1)
O1−Mn1−O1^i	180.000(1)	O8−Mn1−O4	88.0(2)
O8^i−Mn1−O1	89.4(2)	O8−Mn1−O1	90.6(2)
O4^i−Mn1−O1	89.0(2)	O4−Mn1−O1	91.0(2)
O8−Mn1−O4^i	92.0(2)	O1−Mn2−O2	57.1(2)
O3−Mn2−O6	94.2(3)	O3−Mn2−O7	107.7(3)
O3−Mn2−O5	84.9(3)	O7−Mn2−O6	93.1(3)
O6−Mn2−O5	176.5(3)	O7−Mn2−O5	84.0(4)
O7−Mn2−O1	150.4(3)	O3−Mn2−O1	96.6(2)
O5−Mn2−O1	81.5(3)	O6−Mn2−O1	102.0(2)
O7−Mn2−O2	96.3(3)	O3−Mn2−O2	153.1(3)
O5−Mn2−O2	85.7(3)	O6−Mn2−O2	96.5(2)
Mn1−O1−Mn2	107.2(2)		

[a] Symmetry operations in **1**: i, 0.5 − x, 1.5 − y, 1 − z.

(Figure 1a). The Mn1 center is surrounded by six carboxylate oxygen atoms to form octahedral coordination. The equatorial plane is constructed by four carboxylate oxygen atoms (O4, O4A, O8, and O8A) from four different btdc ligands. O4 and O8 are crystallographically equivalent to O4A and O8A, respectively. The axial positions are occupied by two carboxylate oxygen atoms (O1 and O1A) from another two crystallographically equivalent btdc ligands. Mn2 is six-coordinated by coordination to six oxygen atoms (O1, O2, O3, O5, O6, and O7) to form a

Table 3. Select Bond Lengths [Å] and Angles [deg] for Crystal 2

Co1−O1	2.372(2)	Co1−O4	2.008(1)
Co1−O6	2.023(2)	Co1−O5	2.024(2)
Co1−O2	2.024 (1)		
O1−Co1−O4	91.68(6)	O1−Co1−O6	156.49(5)
O4−Co1−O6	107.98(6)	O1−Co1−O5	91.68(6)
O4−Co1−O5	97.70(6)	O6−Co1−O5	98.12(7)
O1−Co1−O2	59.55(5)	O4−Co1−O2	141.58(6)
O6−Co1−O2	97.05(6)	O5−Co1−O2	107.29(6)

Table 4. Select Bond Lengths [Å] and Angles [deg] for Crystal 3

Zn1−O3	1.977(2)	Zn1−O1	1.991(2)
Zn1−O5	1.999(3)	Zn1−O6	2.011(2)
Zn1−O2	2.471(2)		
O3−Zn1−O1	138.78(9)	O3−Zn1−O5	99.1(1)
O1−Zn1−O5	107.91)	O3−Zn1−O6	108.5(1)
O1−Zn1−O6	97.6(1)	O5−Zn1−O6	99.1(1)
O3−Zn1−O2	91.04(9)	O1−Zn1−O2	57.72(8)
O5−Zn1−O2	92.9(1)	O6−Zn1−O2	155.0(1)

Table 5. Select Bond Lengths [Å] and Angles [deg] for Crystal 4[a]

Zn1−O2	2.050(2)	Zn1−O1	2.019(2)
Zn1−N1	2.036(3)	Zn1−O4	2.029(2)
Zn1−O3	2.084(2)	Zn1−Zn1^i	2.9962(7)
O2−Zn1−O1	89.6(1)	O2−Zn1−N1	99.9(1)
O1−Zn1−N1	97.6(1)	O2−Zn1−O4	89.4(1)
O1−Zn1−O4	161.6(1)	N1−Zn1−O4	100.6(1)
O2−Zn1−O3	153.8(1)	O1−Zn1−O3	87.4(1)
N1−Zn1−O3	106.3(1)	O4−Zn1−O3	85.5(1)
O2−Zn1−Zn1^i	80.59(7)	O1−Zn1−Zn1^i	77.10(7)
N1−Zn1−Zn1^i	174.71(8)	O4−Zn1−Zn1^i	84.66(7)
O3−Zn1−Zn1^i	73.37(7)		

[a] Symmetry operations in **4**: i, −x, y, 1.5 − z.

highly distorted octahedral geometry. The carboxylate oxygen atoms O1 and O2 are from a chelating carboxylate group in the same btdc ligand, the carboxylate oxygen atoms O3 and O6 are from two different bidentate carboxylate groups, and the two oxygen atoms O5 and O7 are from two coordinated DMF molecules. The equatorial plane in an octahedron formed by Mn2 is decorated by O1, O2, O3, and O7, and the axial positions are occupied by O5 and O6, with a O6−Mn2−O5 angle of 176.5°. The distortion of the octahedron mainly arises from the small angle of the chelating carboxylate group (O1−Mn2−O2, 57.1°). Although the chelating coordination mode in manganese coordination polymers is not as common as that in the zinc system, there are still some reports. For example, Das and Bharadwaj's group reported a series of manganese coordination polymers with chelating carboxylate groups. The O−Mn−O angles are in the range 56.59−58.07°.[16,17] In crystal **1**, the distances

dx.doi.org/10.1021/ic101112b |*Inorg. Chem.* 2011, 50, 3198–3205

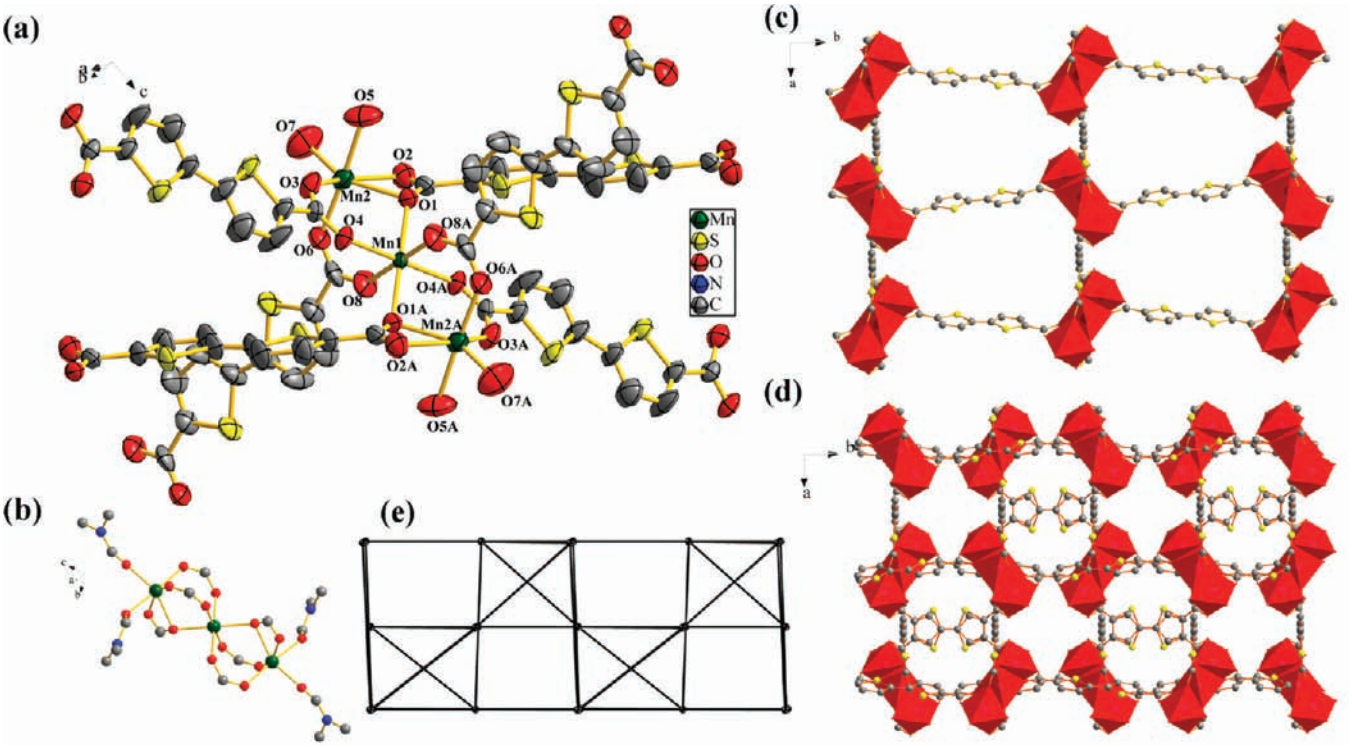

Figure 1. (a) ORTEP drawing of the coordination environments of manganese(II) and the bridging mode of the btdc ligand with ellipsoids at the 50% probability level; all hydrogen atoms and DMF molecules are omitted for clarity. (b) Ball-and-stick representation of $[Mn_3(COO)_6]$ trimetallic clusters in **1**. Schematic representation of (c) a 2D layer and (d) a 3D framework viewed along the *c* axis. (e) Topological view of the framework structure.

Chart 2. Observed Coordination Modes of the btdc Ligands in Crystals 1−4

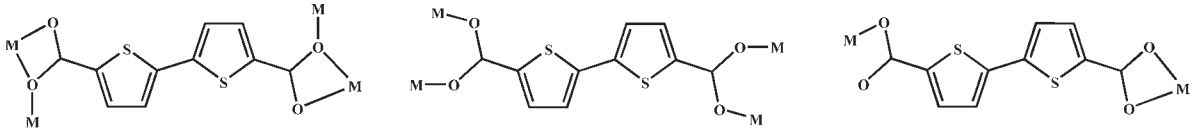

of Mn2−O1 and Mn2−O2 are 2.281(6) and 2.304(6) Å, respectively, which are longer than the common Mn^{II}−O distance of 2.16 Å.[18]

In crystal **1**, the btdc ligands adopt two kinds of coordination modes: A and B (as shown in Chart 2). Two bisbidentate btdc ligands containing a μ_2-O (A) and four bidentate btdc ligands (B) connect Mn1 and crystallographically equivalent Mn2 and Mn2A to form a $[Mn_3(COO)_6]$ trimetallic cluster with DMF molecules acting as terminal ligands fulfilling the coordination spheres (Figure 1b). The Mn1−Mn2 distance is 3.623(1) Å, and the Mn2−Mn1−Mn2 angle is 180°.

The bidentate btdc ligands (B) link trimetallic clusters to stretch into two-dimensional (2D) layers along the *b* axis, as depicted in Figure 1c. These 2D layers are linked by bisbidentate btdc ligands containing a μ_2-O (A) to form a 3D framework viewed along the *c* axis, as shown in Figure 1d. For a topological view, the 3D framework can be simplified by considering the trimetallic clusters as six-connected nodes and the btdc ligands as linkers (Figure 1e).

*Compounds **2** and **3***. Crystals **2** and **3** with similar cell parameters and the same space group $P2_1/c$ are isostructural (Table 1). Hence, only the structure of crystal **3** is described in detail, and the structure description of crystal **2** can be found in the Supporting Information (Figure S1).

Crystal **3** consists of one-dimensional (1D) zigzag polymeric coordination chains, and the building unit is depicted in Figure 2. The building unit contains one zinc(II) ion, one btdc ligand, two coordinated DMF molecules, and one free DMF molecule (Figure 2a). The center zinc atom is five-coordinated through coordination to two oxygen atoms (O1 and O2) from one chelating carboxylate group and one oxygen atom (O3) from the other one monodentate carboxylate group of the btdc ligand, as well as two oxygen atoms (O5 and O6) from two coordinated DMF molecules. It is noted that the Zn1−O4 distance is 2.552(1) Å, suggesting a non-negligible interaction between the zinc atom and the uncoordinated carboxylate oxygen atom. This monodentate carboxylate group here can be described as a semichelating coordination mode, implying a zinc atom in a distorted octahedron environment.[19]

Each btdc ligand, with a monodentate carboxylate group and a bidentate carboxylate group (as shown in Chart 2C), bridges two adjacent zinc atoms to form a 1D infinite zigzag chain (Figure 2b). The angle between ligands is 97.2°, which approaches 90° (Figure 2c).

dx.doi.org/10.1021/ic101112b |*Inorg. Chem.* 2011, 50, 3198–3205

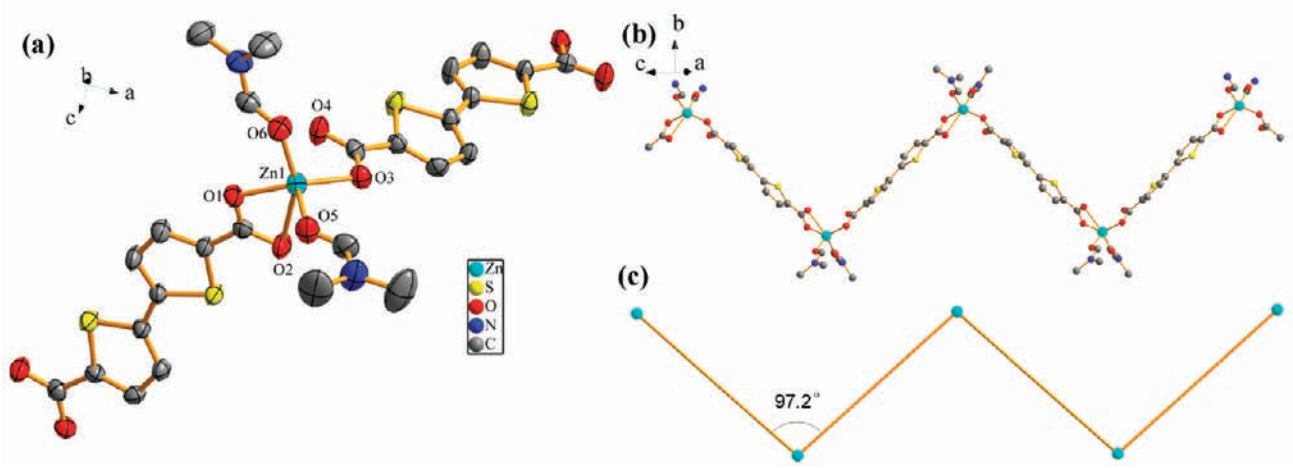

Figure 2. (a) ORTEP drawing of the coordination environments of zinc(II) and the bridging mode of the btdc ligand with ellipsoids at the 50% probability level. All hydrogen atoms and free DMF molecules are omitted for clarity. (b) 1D zigzag polymeric chain in **3**. (c) Schematic representation of the chain.

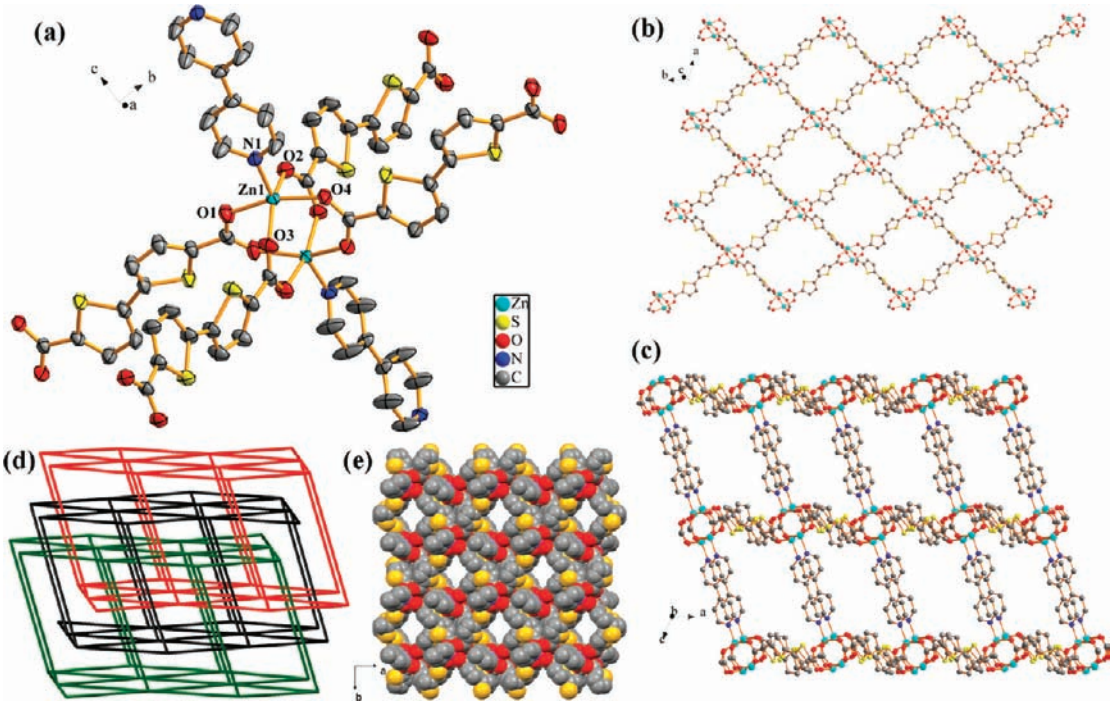

Figure 3. (a) ORTEP drawing of the coordination environments of zinc(II) and the bridging mode of the btdc ligand with ellipsoids at the 50% probability level. All hydrogen atoms are omitted for clarity. (b) 2D square grid. (c) 3D single framework of **4**. (d) Schematic view of the 3-fold interpenetration for **4**. (e) Channel views with a space-filling model along the *c* axis.

Compound ***4***. A single-crystal X-ray analysis reveals that crystal **4** has a 3D framework with 3-fold interpenetration. The building unit contains one zinc(II) atom, one btdc ligand, and a half 4,4′-bpy ligand. Each zinc atom is square-pyramidally coordinated by four carboxylate oxygen atoms (O1, O2, O3, and O4) at the basal positions [Zn1−O (average) 2.045(2) Å] and one 4,4′-bpy nitrogen atom [Zn1−N1 2.036(2) Å] at the apical position (Figure 3a).

Two crystallographically equivalent zinc atoms are bridged by four carboxylate groups from two different btdc ligands adopting a bisbidentate coordination mode (Chart 2B) to generate a well-known paddlewheel second building unit (SBU) with a Zn···Zn separation of 2.996(7) Å. The paddlewheel is bridged by btdc ligands to form a distorted 2D square grid along the *ab* plane (Figure 3b). These 2D square grids are further pillared by 4,4′-bpy molecules, whose nitrogen atoms occupy the axial sites of the paddlewheel subunits, to form a 3D porous structure with large cavities along the *b* axis, as presented in Figure 3c. If the paddlewheel dimers can be topologically viewed as octahedral nodes and the btdc and 4,4′-bpy bridges can be viewed as linkers, the topology of a single net for **4** can be described as an uninodal six-connected distorted primitive cubic net.

dx.doi.org/10.1021/ic101112b |*Inorg. Chem.* 2011, 50, 3198–3205

The large space formed by a single 3D network allows the incorporation of two other identical networks. Therefore, the overall structure of **4** is composed of three identical nets, which interpenetrate each other to form a triply interpenetrating 3D framework (Figure 3d). Hence, the large pore void spaces of a single net have been reduced significantly. Upon interpenetration, the crystal only retains an effective void volume of 621.0 Å^3 per unit cell, which is 17.9% of the crystal volume, calculated by *PLATON* analysis.[20] When viewed along the *c* axis, crystal **4** provides a square channel with dimensions of 3.8 × 3.8 Å (Figure 3e).

Crystals **1**−**3**, synthesized using the same linker (H_2btdc) but different transition-metal connecters, have different structures. Crystal **1** features a 3D infinite framework, and crystals **2** and **3** are composed of 1D zigzag polymeric coordination chains. It is impossible to predict or rationalize the formation of each structure because the outcomes of assembly not only are dependent upon the nature of the metal ion (coordination numbers and geometries) but also are strongly influenced by other factors such as the solvent system and temperature. Crystal **1** was synthesized by the solvothermal method at 100 °C, while crystals **2** and **3** were obtained by the liquid diffusion method at room temperature. It has been proven that the coordination ability of carboxylate is influenced by the temperature.[21] Carboxylate groups tend to form a multidentate coordination mode from higher dimension structures because of higher the reaction temperature. Therefore, the different structures of crystals **1**−**3** are mainly due to the different synthesis temperatures. Crystal **4** using Zn^{2+} as the connector is a 3D network. The 4,4′-bpy ligand used as a linear linker can further pillar the 2D grids formed by the btdc ligand to generate a 3D porous structure.

The thermal stabilities were investigated. For crystal **1**, the preliminary weight loss of 20.57% beginning at ca. 150 °C to ca. 350 °C is attributed to the loss of coordinated DMF molecules (calculated, 24.08%). The following weight loss is from decomposition of the btdc ligand. Crystal **2** loses the free DMF molecule around 200 °C (calculated, 13.78%; found, 13.25%), and the following thermal behavior may be the loss of coordinated DMF molecules and subsequent decomposition of the framework. Crystal **3** has the same decomposition process as crystal **2**. The result of TGA shows that crystal **4** is stable up to ca. 320 °C. Before that temperature, the preliminary weight loss of about 9% is attributed to the loss of solvent molecules contained in the void spaces. There may be two DMF molecules in the unit cell. Then above the temperature, the crystal undergoes rapid decomposition.

3.2. UV/Vis Absorbance Properties. The solid-state UV/vis spectra of H_2btdc and crystals **1**−**4** are displayed in Figure 4. The H_2btdc ligand itself displays strong absorption bands in the UV spectral region from 250 to 450 nm, arising from the $\pi-\pi^*$ transition of the aromatic rings.[22] These bands are not strongly perturbed upon its coordination to manganese(II), cobalt(II), and zinc(II), suggesting that coordination of the metal ions hardly alters the intrinsic electronic properties of H_2btdc. For crystal **1**, the weak shoulder band at wavelengths larger than 450 nm is due to the d−d spin-forbidden transition of the d^5 (Mn^{2+}) ion. For crystal **2**, one clear additional band is observed at 540 nm in addition to the $\pi-\pi^*$ transition band of the btdc ligand, which probably originates from the d−d spin-allowed transition of the d^7 (Co^{2+}) ion. The difference in the UV/vis absorption properties may trace back to a discrepancy in the central metal atoms of the crystals.

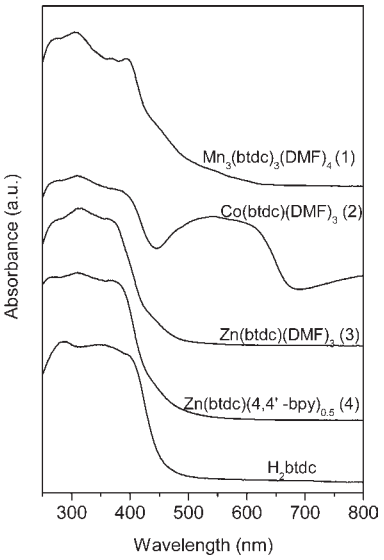

Figure 4. UV/vis diffuse-reflectance spectra of the H_2btdc ligand and crystals **1**−**4** with $BaSO_4$ as the background.

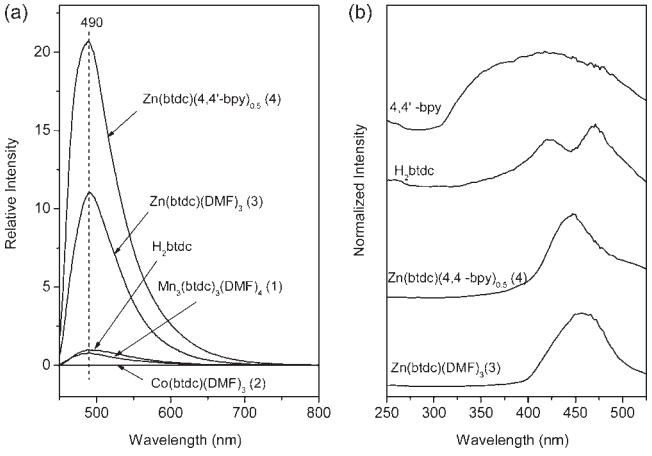

Figure 5. (a) Fluorescent emission spectra of the H_2btdc ligand and crystals **1**−**4** in the solid state at room temperature. (b) Normalized excitation spectra of H_2btdc, 4,4′-bpy, and crystals **3** and **4** in the solid state at room temperature. The excitation spectra are detected at 560 nm.

3.3. Photoluminescent Properties. The solid-state luminescence of crystals **1**−**4** as well as the free H_2btdc ligand was investigated at room temperature. The emission spectra are shown in Figure 5a. All of the emission spectra were measured with a 420 nm excitation source under the same conditions. The H_2btdc ligand shows the emission band centered at about 490 nm. For H_2btdc, the organic ligand with π-conjugated backbones, the emission is usually from the lowest singlet excited state to the singlet ground state. Such transitions are $\pi^*-\pi$ in nature. The emission intensity of crystal **1** is reduced slightly compared with the free H_2btdc ligand. No measurable emission signal is observed for crystal **2**. Crystals **3** and **4** display much stronger emission bands than the free H_2btdc ligand. Strong cyan fluorescent emission can be clearly observed by the eye upon illumination of crystals **3** and **4** with a 420 nm excitation source. This can be further confirmed by the fluorescent images of the

dx.doi.org/10.1021/ic101112b |*Inorg. Chem.* 2011, 50, 3198–3205

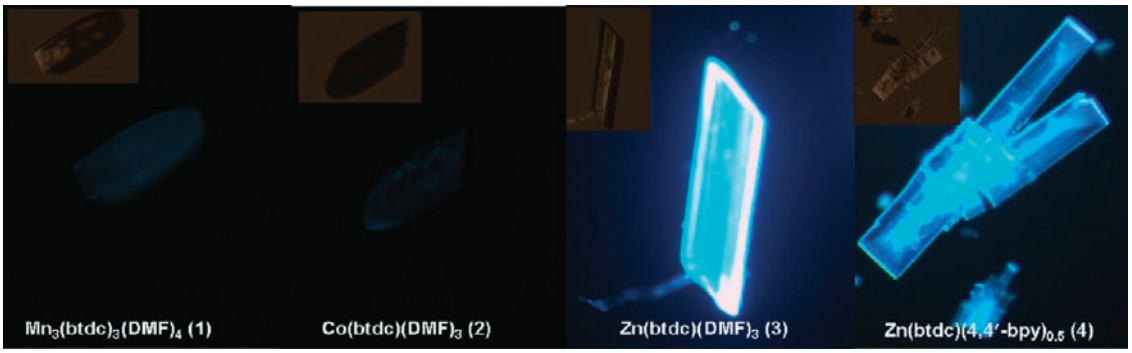

Figure 6. Fluorescent images of crystals **1**−**4** demonstrating changes in the intensity with the metal ions and structures. Inset: bright-field OM images.

crystals (Figure 6). Crystals **1** and **2** only display weak and hardly distinguished images. Strong and bright fluorescent images can be easily observed in the fluorescent images of crystals **3** and **4**.

The emission bands of crystals **1**, **3**, and **4** centered at about 490 nm resemble that of the solid-state H_2btdc ligand. The similarity between the emission spectra of these crystals and the ligand indicates that there is little influence of the metal or metal cluster units on the electronic structure of the linker. This is evidenced by the UV/vis spectra, which clearly show that metal binding does not disturb the detailed electronic structure of the ligand. This gives a clue that the emission of the crystals is essentially ligand-based. Further, the absence of metal-to-ligand and ligand-to-metal charge-transfer bands indicates that the observed emission of crystals is generated solely by the ligand.[3,23−25]

H_2btdc exhibits two excitation bands centered at 423 and 469 nm, as shown in the excitation spectra in Figure 5b. 4,4′-bpy displays a broad excitation band in the range of 310−525 nm. Only one broad excitation band is observed centered at about 450 nm for crystals **3** and **4**. The excitation spectrum of crystal **4** is different from that of powder 4,4′-bpy but very similar to that of crystal **3**, which does not contain 4,4′-bpy in the structure. That is, 4,4′-bpy in the framework does not perturb the electronic structure of btdc significantly; the emission of crystal **4** originates from the btdc ligand.

From Figure 5a, it can be concluded that the luminescence emission of the btdc ligand was severely quenched by coordination with manganese(II) and cobalt(II). The emission from paramagnetic transition-metal complexes is usually not strong because ligand-field transitions (d−d) may lead to strong reabsorption and/or quenching of fluorescence generated from the organic molecule, which can occur via electron or energy transfer through the partially filled d orbitals.[3] These reabsorption and/or quenching effects have also been reported in other MOFs with cobalt, nickel, and manganese metal ions in the literature.[26,27]

The emission intensities of crystals **3** and **4** increase remarkably and are approximately 10 and 20 times that for the free btdc ligand. The zinc(II)-enhanced emission was reported for a variety of linker-based luminescent MOFs. However, the fluorescent intensities of MOFs are generally about 2−3 times greater than that of the free ligand in most cases.[11,26,28] To the best of our knowledge, such a remarkable enhancement was rarely reported for the ligand-based luminescent MOFs. In general, the enhanced fluorescence efficiency is attributed to coordination of the ligand to a zinc(II) ion, which effectively increases the rigidity

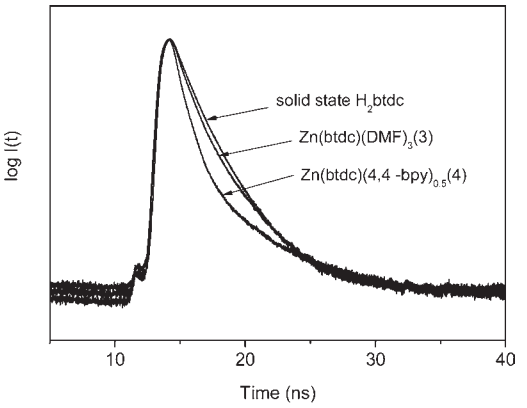

Figure 7. Emission decays of H_2btdc powder and crystals **3** and **4** at room temperature.

of the ligand and reduces thermal vibrations, thereby reducing the nonradiative decay of the intraligand $^1(\pi-\pi^*)$ excited state.[3] The emission intensity of crystal **4** with a 3D condensed polymeric structure is much stronger than that of crystal **3** with a 1D chainlike structure. The more rigid structure of crystal **4** than that of crystal **3** perhaps mainly contributes to the significantly enhanced fluorescent intensity of crystal **4**. These results indicate that both metal ions and structure play important roles in the emission properties of MOFs.

Increased linker rigidity due to metal coordination often reduces the efficiency of nonradiative pathways, which is often accompanied by an increase in the fluorescence lifetimes and quantum yields.[3] Time-resolved emission measurement was investigated, and emission decay curves are shown in Figure 7. Emission decays for the H_2btdc ligand and crystals **3** and **4** are best fit to the biexponential function $I(t) = \alpha_1 e^{-t/\tau_1} + \alpha_2 e^{-t/\tau_2}$, where α_1 and α_2 are normalized preexponential factors ($\alpha_1 + \alpha_2 = 1$) and τ_1 and τ_2 are the short and long lifetimes obtained from the fit, respectively. The lifetimes of the H_2btdc ligand and crystals **3** and **4** are summarized in Table 6. From the free H_2btdc ligand to crystal **3** and to crystal **4**, τ_1 of short-lived species decreases gradually and τ_2 of long-lived species increases sharply. The lifetimes of the long-lived species increase with increasing emission intensity. From previous studies, the short lifetime is probably due to emission from the monomeric ligand and the long-lived species are relative to some excited-state process (i.e., population of the long-lived emissive state occurs after the initial excitation).[10] The results of both the time-resolved emission

dx.doi.org/10.1021/ic101112b |*Inorg. Chem.* 2011, 50, 3198–3205

Table 6. Fluorescence Decay Parameters for H_2btdc and Crystals 3 and 4

	α_1	τ_1 (ns)	α_2	τ_2 (ns)
H_2btdc	0.70	1.06	0.30	2.42
3	0.77	1.03	0.23	3.07
4	0.90	0.69	0.10	6.44

measurement and fluorescent spectra suggest that the greatly enhanced emission intensity may be related to the existence of some highly excited long-lived states in MOFs. From the free H_2btdc ligand to crystal **3** and to crystal **4**, the environment of the btdc ligand is more and more rigid. Therefore, the rigid structure of MOFs can efficiently stabilize the highly excited long-lived states, which can greatly increase the emission intensity of MOFs.

4. CONCLUSIONS

In summary, four metal−organic coordination polymers were successfully synthesized using H_2btdc as the ligand. A 3D infinite framework can be formed using Mn^{2+} as the cation, and Co^{2+} and Zn^{2+} lead to the formation of 1D zigzag polymeric coordination chains. The addition of 4,4′-bpy could help to generate a 3D framework. The crystals display ligand-based emission properties. The luminescence emission of the btdc ligand was severely quenched by coordination with manganese(II) and cobalt(II). An unexpected great enhancement of the emission intensity was observed for the ligands coordinated with Zn^{2+}. The combined results of the time-resolved emission measurement and fluorescent spectra suggest that the greatly enhanced emission intensity may be related to the existence of some highly excited long-lived states in MOFs, which can probably be stabilized by the rigid structure of the btdc ligand. The primary results suggest that structure engineering of the MOFs is a promising strategy to synthesize novel materials with unique photoluminescent properties.

■ ASSOCIATED CONTENT

Ⓢ Supporting Information. X-ray crystallographic files in CIF format, figures of crystal **2**, simulated and experimental PXRD data of crystals **1**−**4**, TGA profiles of crystals **1**−**4**, and ORTEP views of the asymmetric units of crystals **1**−**4**. This material is available free of charge via the Internet at http://pubs.acs.org.

■ AUTHOR INFORMATION

Corresponding Author

*E-mail: yangqh@dicp.ac.cn (Q.-H.Y.), canli@dicp.ac.cn (C.L.). Tel: 86-411-84379552 (Q.-H.Y.), 86-411-84379070 (C.L.). Fax: 86-411-84694447. URL: http://www.hmm.dicp.ac.cn (Q.-H.Y.), http://www.canli.dicp.ac.cn (C.L.).

■ ACKNOWLEDGMENT

The authors are grateful to Dr. Shiming Zhou for refinement of the crystallographic work from Hefei National Laboratory for Physical Sciences at Microscale, University of Science and Technology of China. This work was supported by the Program Strategic Scientific Alliances between China and The Netherlands (Grant 2008DFB50130) and the National Basic Research Program of China (Grant 2009CB623503).

■ REFERENCES

(1) Eddaoudi, M.; Kim, J.; Rosi, N.; Vodak, D.; Wachter, J.; O′Keeffe, M.; Yaghi, O. M. *Science* **2002**, *295*, 469–472.
(2) Murray, L. J.; Dinca, M.; Long, J. R. *Chem. Soc. Rev.* **2009**, *38*, 1294–1314.
(3) Allendorf, M. D.; Bauer, C. A.; Bhakta, R. K.; Houk, R. J. T. *Chem. Soc. Rev.* **2009**, *38*, 1330–1352.
(4) Kurmoo, M. *Chem. Soc. Rev.* **2009**, *38*, 1353–1379.
(5) Dueren, T.; Bae, Y.-S.; Snurr, R. Q. *Chem. Soc. Rev.* **2009**, *38*, 1237–1247.
(6) Lee, J.; Farha, O. K.; Roberts, J.; Scheidt, K. A.; Nguyen, S. T.; Hupp, J. T. *Chem. Soc. Rev.* **2009**, *38*, 1450–1459.
(7) Fang, Q. R.; Zhu, G. S.; Jin, Z.; Xue, M.; Wei, X.; Wang, D. J.; Qiu, S. L. *Angew. Chem., Int. Ed.* **2006**, *45*, 6126–6130.
(8) Xamena, F.; Corma, A.; Garcia, H. *J. Phys. Chem. C* **2007**, *111* 80–85.
(9) Mahata, P.; Madras, G.; Natarajan, S. *J. Phys. Chem. B* **2006**, *110*, 13759–13768.
(10) Bauer, C. A.; Timofeeva, T. V.; Settersten, T. B.; Patterson, B. D.; Liu, V. H.; Simmons, B. A.; Allendorf, M. D. *J. Am. Chem. Soc.* **2007**, *129*, 7136–7144.
(11) Chen, Z. F.; Xiong, R. G.; Zhang, J.; Chen, X. T.; Xue, Z. L.; You, X. Z. *Inorg. Chem.* **2001**, *40*, 4075–4077.
(12) Gunes, S.; Neugebauer, H.; Sariciftci, N. S. *Chem. Rev.* **2007**, *107*, 1324–1338.
(13) Demessence, A.; Rogez, G.; Welter, R.; Rabu, P. *Inorg. Chem.* **2007**, *46*, 3423–3425.
(14) Jia, H. P.; Li, W.; Ju, Z. F.; Zhang, J. *Eur. J. Inorg. Chem.* **2006**, 4264–4270.
(15) Ni, Z.; Yassar, A.; Antoun, T.; Yaghi, O. M. *J. Am. Chem. Soc.* **2005**, *127*, 12752–12753.
(16) Das, M. C.; Bharadwaj, P. K. *J. Am. Chem. Soc.* **2009**, *131*, 10942–10949.
(17) Das, M. C.; Bharadwaj, P. K. *Chem.—Eur. J.* **2010**, *16*, 5070–5077.
(18) Chen, X. M.; Cai, J. W. *Single-Crystal Structural Analysis—Principles and Practices*; Science Press: Beijing, China, 2007.
(19) Sun, Q.; Yue, Q.; Zhang, J. Y.; Wang, L.; Li, X.; Gao, E. Q. *Cryst. Growth Des.* **2009**, *9*, 2310–2317.
(20) Spek, A. L. *J. Appl. Crystallogr.* **2003**, *36*, 7–13.
(21) Livage, C.; Egger, C.; Ferey, G. *Chem. Mater.* **2001**, *13*, 410–414.
(22) Zhou, Y. X.; Shen, X. Q.; Du, C. X.; Wu, B. L.; Zhang, H. Y. *Eur. J. Inorg. Chem.* **2008**, 4280–4289.
(23) Song, X. Q.; Liu, W. S.; Dou, W.; Wang, Y. W.; Zheng, M. R.; Zang, Z. P. *Eur. J. Inorg. Chem.* **2008**, 1901–1912.
(24) Dai, J. C.; Wu, X. T.; Fu, Z. Y.; Cui, C. P.; Hu, S. M.; Du, W. X.; Wu, L. M.; Zhang, H. H.; Sun, R. O. *Inorg. Chem.* **2002**, *41*, 1391–1396.
(25) Fan, J.; Zhu, H. F.; Okamura, T. A.; Sun, W. Y.; Tang, W. X.; Ueyama, N. *New J. Chem.* **2003**, *27*, 1409–1411.
(26) Lu, Z. D.; Wen, L. L.; Ni, Z. P.; Li, Y. Z.; Zhu, H. Z.; Meng, Q. J. *Cryst. Growth Des.* **2007**, *7*, 268–274.
(27) Fang, Z. L.; Yu, R. M.; He, J. G.; Zhang, Q. S.; Zhao, Z. G.; Lu, C. Z. *Inorg. Chem.* **2009**, *48*, 7691–7697.
(28) Li, M.; Xiang, J. F.; Yuan, L. J.; Wu, S. M.; Chen, S. P.; Sun, J. T. *Cryst. Growth Des.* **2006**, *6*, 2036–2040.